Hydrogen-Transferred Radical Cations of NADH Model Compounds. 2. Sequential Electron−Proton Addition to NAD^+

Andrzej Marcinek,* Jacek Rogowski, Jan Adamus, and Jerzy Gębicki*

Institute of Applied Radiation Chemistry, Technical University, 90-924 Lodz, Poland

Paweł Bednarek[†] and Thomas Bally*

Institute of Physical Chemistry, University of Fribourg, Perolles, CH-1700 Fribourg, Switzerland

Received: October 27, 1999

Sequential electron−proton addition to different NAD^+ model compounds was studied by pulse radiolysis. Under mildly acidic conditions, the radicals obtained by reduction of the cations are protonated at the carbonyl group. The pK_a values of the resulting enol radical cations were determined. The same enol radical cations can also be formed via a deprotonation−reprotonation process from the keto radical cations of the corresponding NADH model compounds.

1. Introduction

In ref 1, we demonstrated that on oxidation of NADH model compounds, **XHK**, the tautomeric enol radical cations, $\mathbf{XHE}^{\bullet+}$, may form spontaneously, provided that the carbonyl group assumes a favorable orientation for the required [1,4]-hydrogen atom transfer. In this paper we show that the same species $\mathbf{XHE}^{\bullet+}$ are also formed upon protonation of radicals, $\mathbf{X}^{\bullet}$, which can be obtained by the reduction of NAD^+ model compounds, $\mathbf{X}^+$. This approach is more general, since the geometric requirements are less important than in the case of the intramolecular $\mathbf{XHK}^{\bullet+} \rightarrow \mathbf{XHE}^{\bullet+}$ tautomerization described in ref 1. When this latter process is ineffective because of structural or environmental reasons, deprotonation is a major decay path for keto radical cations, $\mathbf{XHK}^{\bullet+}$. However, in these cases reprotonation of the radicals may lead to the more stable enol radical cations, $\mathbf{XHE}^{\bullet+}$. We believe that these studies contribute to a better understanding of mechanism of the NADH ⇄ NAD^+ transformation.

SCHEME 1

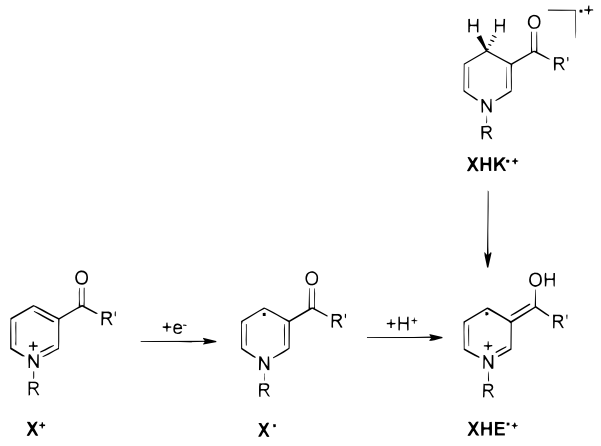

[†] On leave from the Institute of Applied Radiation Chemistry, Technical University, 90-924 Lodz, Poland.

2. Results and Discussion

Model Compounds. We have chosen for this study the oxidized forms of 1,4-dihydropyridines that were discussed in ref 1: $\mathbf{1}^+$ [the oxidized form of 1-methyl-1,4-dihydro-6,7,8,9-tetrahydro-5*H*-cyclohepta[b]pyridin-5-one, (**1HK**)], $\mathbf{2}^+$ [the oxidized form of 1-methyl-1,4,7,8-tetrahydro-5(6*H*)-quinolinone (**2HK**)], and $\mathbf{3}^+$ [the oxidized form of 1-methyl-3-formyl-1,4-dihydropyridine (**3HK**)]. In addition, $\mathbf{4}^+$ [the oxidized form of 1-benzyl-3-acetyl-1,4-dihydropyridine (**4HK**)] was also investigated. In the first step, radicals $\mathbf{X}^{\bullet}$ are formed by reduction of

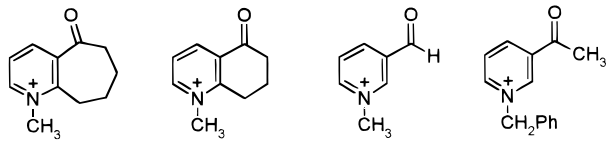

the corresponding cations $\mathbf{X}^+$, whereas in the second step the radicals are protonated to form enol radical cations $\mathbf{XHE}^{\bullet+}$ [Scheme 1]. Spectroscopic and kinetic characterization of the different species involved in these processes will be presented.

Sequential Electron−Proton Addition. Electron addition to $\mathbf{1}^+$ was achieved by pulse radiolytic reduction in aqueous solution at room temperature.[2−5] The spectrum obtained at pH 7 (Figure 1A, curve a) has a maximum at 490 nm and an elevated absorption below 340 nm. Reduction of $\mathbf{1}^+$ to $\mathbf{1}^{\bullet}$ could also be achieved by electron radiolysis in 2-propanol at 77 K (Figure 1B),[6] which resulted in a spectrum similar to that obtained at pH 7 in aqueous solution.

At pH 3 (Figure 1A, curve b) a spectrum that clearly corresponds to a different species is obtained. Monitoring the absorption of the radical $\mathbf{1}^{\bullet}$ at 500 nm as a function of pH gave the titration curve shown as an inset to Figure 1A. It indicates that the radical is being protonated at lower pH. The time dependence of the absorption at 500 nm followed, for example, at pH 4.5 (see inset to Figure 2) shows a rapid decay to a level that remains constant on the microsecond time scale. This means that after protonation of a fraction of $\mathbf{1}^{\bullet}$ [the initial spectrum collected 45 ns after a pulse (curve a in Figure 2) is dominated

10.1021/jp993816z CCC: $19.00
Published on Web 01/07/2000

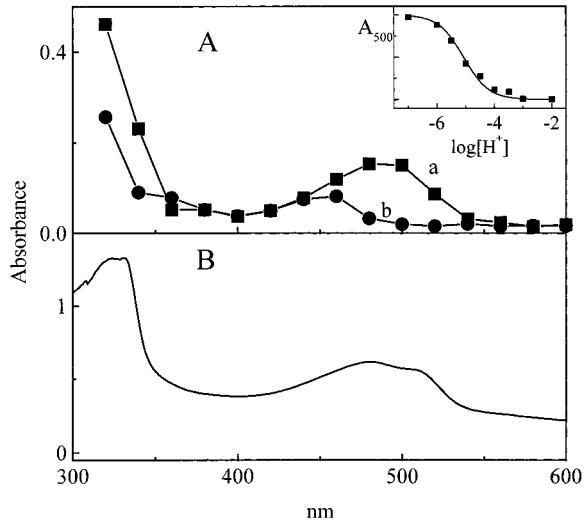

Figure 1. Transient absorption spectra observed upon radiolysis. (A) $\mathbf{1}^+$ (3×10^{-3} M) in aqueous solution (N_2O, 2-propanol [1 M]): dose, 50 Gy; thickness of the sample, 1 cm; $T = 25$ °C; spectra collected 2×10^{-7} s after a 17 ns pulse at pH 7 (a) and pH 3 (b). Inset: absorption (arbitrary units) at 500 nm (after 4×10^{-6} s) vs pH. (B) $\mathbf{1}^+$ (saturated solution) in 2-propanol matrix (77 K): dose, 10 kGy; thickness of the sample, 3 mm.

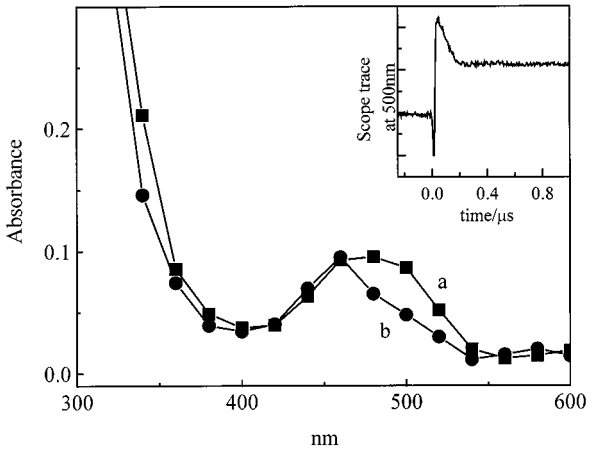

Figure 2. Transient absorption spectra obtained by pulse radiolysis of $\mathbf{1}^+$ (3×10^{-3} M) in aqueous solution (N_2O, 2-propanol [1 M], pH 4.5): dose, 50 Gy; thickness of the sample, 1 cm; $T = 25$ °C. Spectra were collected 4.5×10^{-8} s (a) and 2×10^{-7} s (b) after a 17 ns pulse. Inset: scope trace at 500 nm.

by the radical absorption] an equilibrium is achieved (curve b in Figure 2 shows a mixture of $\mathbf{1}^\bullet$ and $\mathbf{1HE}^{\bullet+}$).

Since the keto radical cation $\mathbf{XHK}^{\bullet+}$, which is obtained by protonation at C-4, is less stable than the corresponding enol form $\mathbf{XHE}^{\bullet+}$, which arises upon O protonation,[1] it is reasonable to assume that the latter is being formed predominantly. Indeed, $\lambda_{max} = 460$ nm of the species that is obtained from $\mathbf{1}^\bullet$ agrees very well with the peak at 453 nm in the spectrum of $\mathbf{1HE}^{\bullet+}$ observed after intramolecular H transfer from $\mathbf{1HK}^{\bullet+}$ in argon matrices[1] (the band system of $\mathbf{1HE}^{\bullet+}$ at 700−900 nm lies outside the observation range of the present experiments).

Similar conclusions were reached for the other two compounds (see Figure 3). From the titration curves we deduce pK_a values of 5.1 ± 0.1 for $\mathbf{1HE}^{\bullet+}$, 4.3 ± 0.1 for $\mathbf{3HE}^{\bullet+}$, and 4.5 ± 0.1 for $\mathbf{4HE}^{\bullet+}$. These values are about 3 units higher than those of enol radical cations generated from NADH analogues carrying an amide group,[2,7] which testifies to the inductive effect of the NH_2 group in these compounds.

To confirm the assignment of the spectra to the radicals obtained by reduction, we carried out CASSCF/CASPT2

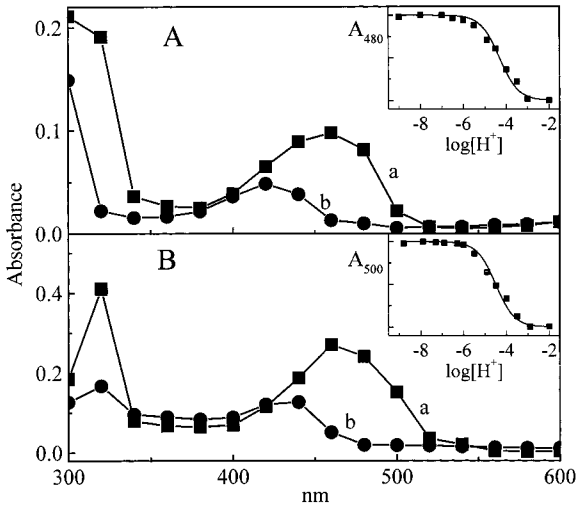

Figure 3. Transient absorption spectra observed upon pulse radiolysis. (A) $\mathbf{3}^+$ (3×10^{-3} M) in aqueous solution (N_2O, 2-propanol [1 M]), with spectra collected 1.2×10^{-6} s after a 17 ns pulse at pH 7 (a) and pH 3 (b): dose, 50 Gy; thickness of the samples, 1 cm; $T = 25$ °C. Inset: absorption (arbitrary units) at 480 nm (after 4×10^{-6} s) vs pH. (B) $\mathbf{4}^+$ (1×10^{-2} M) in aqueous solution (N_2, 2-propanol [0.1 M]), with spectra collected 3.6×10^{-7} s after a 17 ns pulse at pH 7 (a) and pH 3 (b): dose, 50 Gy; thickness of the samples, 1 cm; $T = 25$ °C. Inset: absorption (arbitrary units) at 500 nm (after 5×10^{-7} s) vs pH.

TABLE 1: Excited States of $\mathbf{3}^\bullet$ by CASPT2 Calculations

states	EAS, nm	CASPT2, nm	f^a	CASSCF configurations^b
$1^2A''$	(0)	(0)		81% $(\pi_6)^1$ (ground state)
$2^2A''$		1277	0.003	78% $\pi_6 \rightarrow \pi_7^*$
$3^2A''$	460	422	0.027	48% $\pi_6 \rightarrow \pi_8^*$
				16% $\pi_4 \rightarrow \pi_6$
$4^2A''$	<320	289	0.029	57% $\pi_5 \rightarrow \pi_6$
$5^2A''$		278	0.134	33% $\pi_5 \rightarrow \pi_6$
				26% $\pi_6 \rightarrow \pi_8^*$

[a] Oscillator strength for electronic transition. [b] Active space: 11 electrons in 5 occupied + 6 virtual a″ MOs. In terms of excitations within the π-MOs (π_6 is the HOMO).

calculations for $\mathbf{3}^\bullet$ (Table 1). These show that the band with $\lambda_{max} = 460$ nm corresponds to the *second* excited state (the HOMO → LUMO excitation in the NIR cannot be detected in the present experiments). The observed transition, which corresponds to a mixture of excitations within the occupied MOs and into virtual MOs, is predicted to be ∼0.25 eV too high in energy. The reason for this may be the increase in the dipole moment from 2.76 to 3.76 D on excitation (CASSCF prediction). In aqueous solution this increase is expected to result in significantly enhanced solvation of the second excited state, i.e., in a red shift of the corresponding absorption band.

Protonation of $\mathbf{3}^\bullet$ leads to a band with $\lambda_{max} = 420$ nm. This band could not be observed in the previous argon matrix experiments because it was obscured by absorptions of neutral **3HK**, which do not intervene under the present conditions. We note, however, that its position is in excellent agreement with the CASPT2 prediction of $\lambda_{max} = 435$ nm for the second excited state of $\mathbf{3HE}^{\bullet+}$.[1] Also, the blue shift of 30 nm on going from $\mathbf{1HE}^{\bullet+}$ to $\mathbf{3HE}^{\bullet+}$ is well reproduced by TD-B3LYP calculations (reported in Table 6 of ref 1).

In all cases protonation is so rapid that it is obscured by reduction of cation. The electron capture rate can be significantly enhanced by raising the concentration of the salt. Nevertheless, the rate of protonation can only be estimated as $>10^{-10}$ M^{-1} s^{-1}. However a primary kinetic isotope effect of $k_{H_2O}/k_{D_2O} = 2.7$ could be determined (measured for $\mathbf{4}^+$); i.e., the lifetime of the radical increases in deuterated water. At equilibrium the

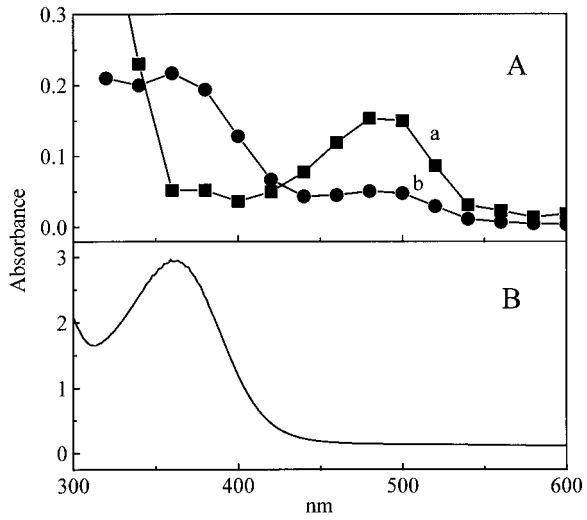

Figure 4. Absorption spectra obtained by pulse radiolysis of $\mathbf{1}^+$ (3×10^{-3} M) in aqueous solution (N_2O, 2-propanol [1 M], pH 7) at dose of 50 Gy, thickness of the sample of 1 cm, and $T = 25$ °C: (A) spectra collected 2×10^{-7} s (a) and 7×10^{-5} s (b) after a 17 ns pulse; (B) steady-state spectrum detected a few minutes after delivering a radiation dose of 750 Gy.

SCHEME 2

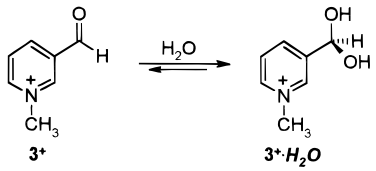

radical absorption is lower in D_2O, which can be explained by the slightly higher acidity of D_3O^+.[8]

For $\mathbf{3}^+$ only, a slower reduction process is observed (at least about an order of magnitude). The lower reactivity of $\mathbf{3}^+$ toward electrons (also, $\mathbf{3}^+$ cannot be reduced in alcoholic matrices) may be explained by hydration of this cation in aqueous solution [Scheme 2].[9,10]

Since electron capture takes place at the O atom,[2,7] such a hydration could be the reason for the observed retardation of the reduction. However, after the reduction of $\mathbf{3}^+ \cdot H_2O$ is completed, the ensuing products, i.e., $\mathbf{3}^\bullet$ and $\mathbf{3HE}^{\bullet+}$, show spectroscopic and kinetic features similar to those observed in the case of $\mathbf{1}^+$ and $\mathbf{4}^+$ (see Figures 1 and 3). This indicates that (if H_2O is present) reduction of $\mathbf{3}^+ \cdot H_2O$ is followed by immediate dehydration and that the further reactivity is analogous to that of $\mathbf{1}^+$.

After the equilibrium between $\mathbf{1}^\bullet$ and $\mathbf{1HE}^{\bullet+}$ is reached, both species decay in a parallel fashion following second-order kinetics $2k/(\epsilon l) = (3-5) \times 10^4$ s^{-1}. Thereby a new product with an absorption around 360−380 nm is formed (Figure 4A). This absorption was assigned to the dimer $\mathbf{1}-\mathbf{1}$.[2−5] In neutral or basic solution $\mathbf{1}-\mathbf{1}$ was stable enough to be observed for several minutes after radiolysis by a steady-state method (Figure 4B).

Deprotonation−Reprotonation Reactions of Ionized NADH Model Compounds. In organic low-temperature matrices ionization of different NADH model compounds leads to formation of the parent keto radical cations, which under those conditions do not undergo enolization.[1,11] In the rigid matrix environment no changes in the spectra were observed even after several hours, and illumination of the samples did not result in any spectral changes except for slow photobleaching of the primary radical cation absorption presumably through charge recombination.

However, we now found that significant changes become noticeable on matrix annealing that promotes slow diffusion leading to intermolecular processes. All four NADH analogues **1HK**−**4HK** exhibit a similar pattern of reactivity on annealing after ionization. We will illustrate this for 1-methyl-1,4,7,8-tetrahydro-5(6*H*)-quinolinone, **2HK**, because in this compound

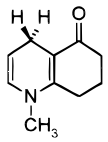

2HK

conformational changes can be neglected and no spontaneous intramolecular tautomerization is observed in the corresponding radical cation.[1]

In the absence of intramolecular enolization, deprotonation is found to be a major decay path of radical cations generated from NADH model compounds.[12] In pulse radiolysis experiments conducted in aqueous solutions of **2HK**, the lifetime of the radical cation increases with decreasing concentration of the starting material, which indicates that the neutral substrate can act as a proton acceptor.[13−15] The rate constant for

$$\mathbf{2HK}^{\bullet+} + \mathbf{2HK} \rightarrow \mathbf{2}^\bullet + \mathbf{2H_2}^+$$

was found to be 2.5×10^9 M^{-1} s^{-1}.

A strong absorption of $\mathbf{2H_2}^+$ overlaps with the absorption band of neutral **2HK**, but its assignment was confirmed experimentally. Pulse radiolysis of a 1:1 mixture of CH_2Cl_2 and CH_3CN generates HCl,[14,15] which protonates **2HK** and leads to a species with an absorption below 450 nm that decays within milliseconds under these experimental conditions.

In a 2-chlorobutane matrix the first product that can be spectroscopically distinguished on annealing to 95 K also absorbs below 450 nm. Because of strong overlap of this band with that of the neutral precursor, its rise manifests itself as a red shift of the **2HK** absorption. These changes are accompanied by the decay of the radical cation absorption (see Figure 5A, curves a and b) and can be interpreted as deprotonation of $\mathbf{2HK}^{\bullet+}$ and formation of $\mathbf{2H_2}^+$. Only a very weak absorption band, which can be assigned to the radical $\mathbf{2}^\bullet$, is seen most likely because the oscillator strength for this transition is much smaller.

Prolonged annealing of the matrix to 107 K leads to a further decay of the radical cation with distinct formation of a new group of absorption bands in the region 450−500 nm, along with a further increase of the absorption below 450 nm (Figure 5A, curve c). These bands can be assigned to the radical $\mathbf{2}^\bullet$, obtained on deprotonation of $\mathbf{2HK}^{\bullet+}$, as similar bands are observed upon one-electron reduction of the corresponding cation, $\mathbf{2}^+$, embedded in a methanol matrix (Figure 5C). The assignment to $\mathbf{2}^\bullet$ is also in accord with that of the spectra in Figures 1 and 3 assigned to the related radicals $\mathbf{1}^\bullet$, $\mathbf{3}^\bullet$, and $\mathbf{4}^\bullet$. A sequence of a strong narrow absorption band at around 500 nm with a broader shoulder at shorter wavelength is observed under matrix conditions for $\mathbf{3}^\bullet$ and $\mathbf{4}^\bullet$ also (see Figure 6) and is reminiscent of the acridinyl radical.[16−18]

However, we cannot exclude the possibility that, along with the radical $\mathbf{2}^\bullet$, the enol radical cation $\mathbf{2HE}^{\bullet+}$ is also formed. It is possible that if the basicity of the radical is sufficient, it may be protonated to give the corresponding enol radical cation. **2HK** is a good model substrate to analyze this problem because in this case the absorption bands of the radical and the enol radical

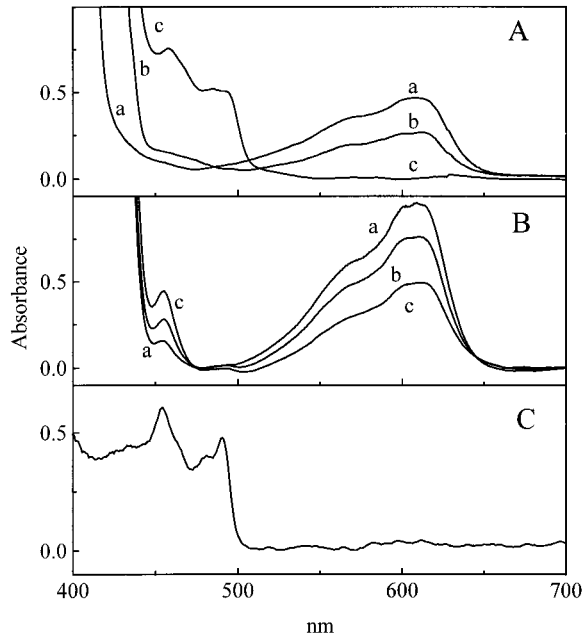

Figure 5. Transient absorption spectra observed upon radiolysis. (A) **2HK** (2×10^{-2} M) in 2-chlorobutane matrix: dose, 7 kGy; thickness of the sample, 2 mm. Spectra were collected at 77 K (a), after thermal relaxation of the sample at 95 K for 10 min (b), and at 107 K for 10 min (c). (B) **2HK** (1×10^{-2} M) in 2-chlorobutane matrix: dose, 20 kGy; thickness of the sample, 3 mm. Spectra were collected after thermal relaxation of the sample at 100 K for 10 min (a), 20 min (b), and 25 min (c). (C) $\mathbf{2}^+$ (5×10^{-3} M) in methanol matrix (77 K): dose, 20 kGy; thickness of the sample, 2 mm.

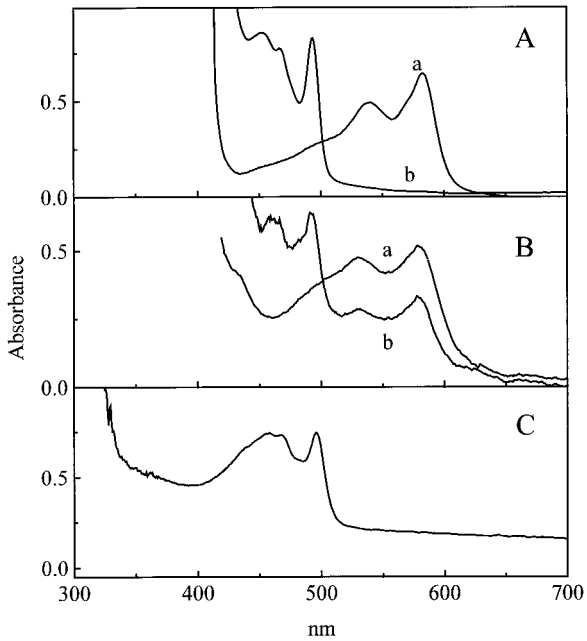

Figure 6. Transient absorption spectra observed upon radiolysis. (A) **3HK** (1×10^{-2} M) in 2-chlorobutane matrix: dose, 10 kGy; thickness of the sample, 3 mm. Spectra were collected at 77 K (a) and after thermal relaxation of the sample at 105 K for 15 min (b). (B) **4HK** (saturated solution) in 2-chlorobutane matrix: dose, 14 kGy; thickness of the sample, 2 mm. Spectra were collected at 77 K (a) and after thermal relaxation of the sample at 100 K for 20 min (b). (C) $\mathbf{4}^+$ (5×10^{-3} M) in 2-propanol matrix (77 K): dose, 16 kGy; thickness of the sample, 3 mm.

cation are clearly separated and no conformational changes interfere with the spectroscopic analysis.

Selective photobleaching experiments demonstrated indeed that the two bands in Figure 5A, curve c, belong to different species. Also, when the rate of annealing was changed, these two species were formed in a different ratio and, moreover, they decayed with different rates on further thermal relaxation of the matrix. In the first experiment (Figure 5A) both species arose simultaneously, whereas in the second experiment (Figure 5B) almost none of the radical absorbing at 490 nm was observed, while the transformation of the primary radical cation into a product absorbing at 455 nm still occurred. This product can be assigned to the enol radical cation, $\mathbf{2HE}^{\bullet+}$, but because it is generated only upon matrix softening, where diffusion is allowed, it must be formed via an intermolecular process.

Two possible reactions may be responsible for the formation of the enol radical cation both of which are energetically feasible according to B3LYP/6-31G* calculations and involve the neutral radical as a key intermediate (see Scheme 3). As the concentration of the radical increases (reaction 1), it begins to compete (by virtue of its higher basicity) with the neutral compound in the deprotonation of the keto radical cation (reaction 2), although electron transfer (reaction 3) seems to be more favorable in this case. [5,19−21]

On the other hand, the products of the initial hydrogen-transfer step (reaction 1) are formed close to one another under matrix conditions. Furthermore, under conditions of slow diffusion, any exchange of reactants, as is required for reactions 2 and 3 or for dimerization of radicals, is significantly inhibited. Thus, hydrogen back-transfer, which is also exothermic if it leads to the enol radical cation (reaction 4), may take over. In this mechanism, enolization of the initial keto radical cation may be considered as being assisted or catalyzed by the neutral keto compound, which acts as a proton shuttle.

3. Conclusions

The results presented in this paper clearly indicate that a stepwise electron−proton−electron transfer in NADH $\rightleftarrows$ NAD^+ type transformations necessarily involves two tautomeric forms of the NADH radical cation (Scheme 4). In particular, the reverse stepwise transformation of NAD^+ to NADH occurs by protonation of the $NAD^{\bullet}$ radical at the oxygen atom, which leads to the more stable enol radical cation. After reneutralization, the enol form reverts rapidly to the more stable keto form of NADH, thus closing the cycle of reactions.

4. Experimental Section

Compounds. 1-Benzyl-3-acetyl-1,4-dihydropyridine (4HK). A solution of 3-acetylpyridine (Aldrich, 3 g, 25 mmol) and benzyl chloride (3.5 g, 30 mmol) in 10 mL of anhydrous methanol was refluxed for 3 h. The solvent was distilled under vacuum and the residual solid washed with ethyl ether and vacuum-dried to give 5.8 g (92%) of 1-benzyl-3-acetylpyridinium chloride ($\mathbf{4}^+$). **4HK** was obtained by dithionite reduction of $\mathbf{4}^+$ according to the literature prescription[22] and purified by column chromatography (silica gel, $CHCl_3$) and then crystallized from petroleum ether (mp 65−66 °C). ^{1}H NMR (80 MHz, $CHCl_3$) δ ppm: 2.09 (s, 3H, CH_3), 2.98 (m, 2H, CH_2), 4.49 (s, 2H, CH_2−Ph), 4.85 (m, 1H), 5,92 (m, 1H), 7.37 (m, 5H, C_6H_5), 7.40 (s, 1H).

The syntheses of other oxidized and reduced compounds are described in ref 1.

Radiolysis in Solution. The pulse radiolysis of water produces three highly reactive species: $H_2O \rightarrow e_{aq}$ (2.6), $^{\bullet}OH$ (2.7), and $H^{\bullet}$ (0.6) (numbers in parentheses are the *G* values, i.e., yield of radicals per 100 eV of energy absorbed).[23]

The radicals of interest are mainly formed by the reaction of pyridine salts with e_{aq} with a rate greater than 10^{10} M^{-1} s^{-1}. To study this reaction without any interference of the other products

SCHEME 3: Energy Changes in kcal/mol from B3LYP/6-31G* Calculations on Fully Optimized Geometries

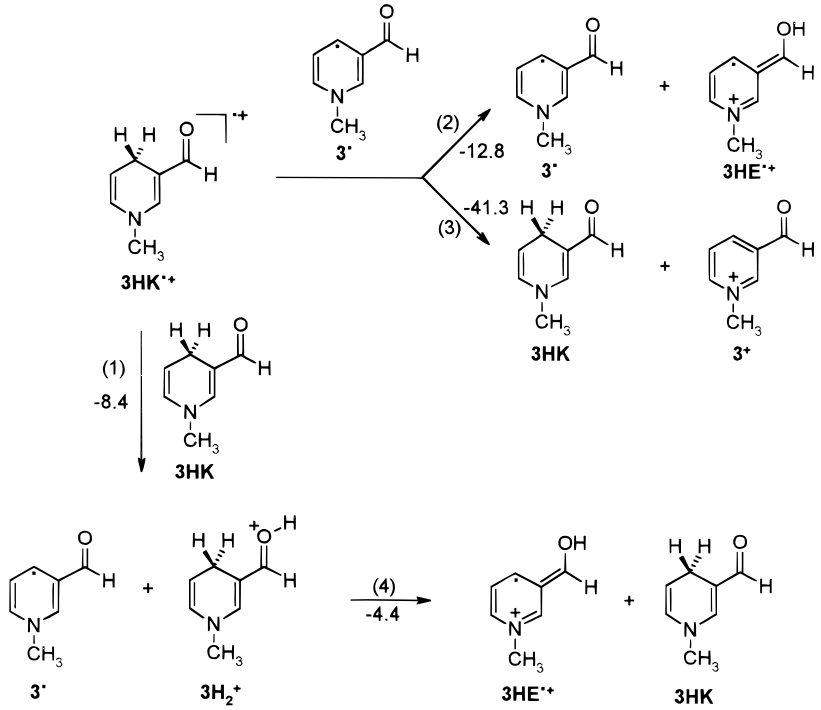

SCHEME 4

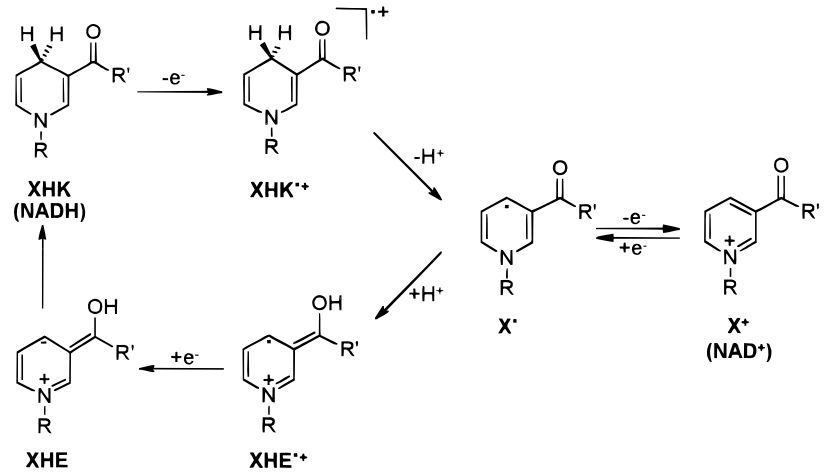

from the radiolysis of water, it is necessary to scavenge the •OH radicals by *tert*-butyl or isopropyl alcohols (0.1−1 M) in the N_2-saturated aqueous solutions. Isopropanol also effectively scavenges H• atoms.[24,25]

The radical produced from the reaction of •OH with *tert*-butyl alcohol is inert in further reactions, but the acetone ketyl radical formed via the following reactions

$$^{\bullet}OH + (CH_3)_2CHOH \rightarrow (CH_3)_2{}^{\bullet}COH + H_2O \qquad (5)$$

$$^{\bullet}H + (CH_3)_2CHOH \rightarrow (CH_3)_2{}^{\bullet}COH + H_2 \qquad (6)$$

acts as an reducing agent. This enables a quantitative analysis of results over a wide pH range, since •OH radicals and H• atoms are converted to a reducing agent, i.e., acetone ketyl radical. It is especially important in acidic solutions when most of the electrons are captured by protons, lowering the yield of the electron attachment products. Because the $(CH_3)_2$•COH radical reacts with solute as a reducing agent in the pH range 1−10, this method was used to determine the pK_a value of the transient species. The rate constant of the reaction of the acetone ketyl radical with solute was found to be $(0.7-1) \times 10^9$ M^{-1} s^{-1}. Complete reduction by the acetone ketyl radical was achieved in aqueous solutions containing 1 M 2-propanol saturated with N_2O, which converts e_{aq} into •OH radicals with a rate constant on the order of 10^{10} M^{-1} s^{-1}.

$$e_{aq} + N_2O \rightarrow {}^{\bullet}OH + OH^- + N_2 \qquad (7)$$

The reactions of one-electron oxidants $Br_2^{\bullet-}$ and N_3• (formed in the reactions shown below) with **2HK** were carried out in N_2O-saturated aqueous solutions of Br^- and NaN_3 (5×10^{-2} M), respectively.[24,25]

$$Br^- + {}^{\bullet}OH \rightarrow {}^{\bullet}Br + OH^- \qquad (8)$$

$$^{\bullet}Br + Br^- \rightarrow Br_2{}^{\bullet-} \qquad (9)$$

$$N_3{}^- + {}^{\bullet}OH \rightarrow N_3{}^{\bullet} + {}^-OH \qquad (10)$$

Solutions were buffered with perchloric acid, potassium hydroxide, and phosphate buffers. The concentration of solute was kept in the range $(1-10) \times 10^{-3}$ M.

The pulse radiolysis system based on a linear electron accelerator delivering a dose of 10−50 Gy per pulse (17 ns) was described earlier.[26]

Experiments in Cryogenic Glasses. 2-Chlorobutane, methylcyclohexane, and 2-propanol or methanol were used as organic matrices, which on freezing form transparent glasses suitable for optical measurements. The samples were prepared by immersing room-temperature solutions in liquid nitrogen. The samples were 2−3 mm thick and were placed in temperature-controlled liquid helium or nitrogen-cooled cryostats (Oxford Instruments). The desired temperature (10−100 K) was achieved by proper helium flow and/or automatically controlled heating. The optical absorption spectra were measured on a Philips 8710 or a Cary 5 (Varian) spectrophotometer.

The samples mounted in a cryostat were irradiated with 4 μs electron pulses from an ELU-6 linear accelerator. Details of the pulse radiolysis system are given elsewhere.[26,27]

Quantum Chemical Calculations. The geometries of all species were optimized by the B3LYP density functional method[28,29] as implemented in the Gaussian 94 suite of programs,[30,31] using the 6-31G* basis set. Relative energies were calculated at the same level.

Excited-state calculation on **3**• was carried out at the B3LYP/6-31G* geometries by the CASSCF/CASPT2 procedure[32] with the MOLCAS program[33] using the [C,N,O]3s2p1d/ [H]2s ANO basis set.[34] The active space was chosen to obtain a satisfactory description of all π excited states of interest at the CASPT2 level (the CASPT2 wave functions are described to 68−72% by the CASSCF wave function for all excited states).

Acknowledgment. This work was supported by grants from the State Committee for Scientific Research (No. 3/T09A/097/11) and Swiss National Science Foundation (No. 2000-053568.98). J.G. thanks the Foundation on behalf of Polish Science for support from the program "Subsidies for Scholars".

Supporting Information Available: Listing of total energies and Cartesian coordinates from the B3LYP calculations for the compounds in Scheme 3 and available in ASCII format through the Internet. This material is available free of charge via the Internet at http://pubs.acs.org.

References and Notes

(1) Marcinek, A.; Adamus, J.; Huben, K.; Gębicki, J.; Bartczak, T. J.; Bednarek, P.; Bally, T. *J. Am. Chem. Soc*., in press.

(2) Brühlmann, U.; Hayon, E. *J. Am. Chem. Soc.* **1974**, *96*, 6169.

(3) Land, E. J.; Swallow, A. J. *Biochim. Biophys. Acta* **1968**, *162*, 327.

(4) Neta, P.; Patterson, L. K. *J. Phys. Chem.* **1974**, *78*, 2211.

(5) Kosower, E. M.; Teuerstein, A.; Burrows, H. D.; Swallow, A. J. *J. Am. Chem. Soc.* **1978**, *100*, 5185.

(6) Some of electrons generated upon radiolysis are stabilized in the matrix, and their absorption may interfere with the absorption of other radiolysis products in the visible region; however, it can be easily bleached photochemically or thermally. It leads to a concomitant increase in the radical absorption, which confirms this assignment.

(7) Tripathi, G. N. R.; Su, Y.; Bentley, J.; Fessenden, R. W.; Jiang, P.-Y. *J. Am. Chem. Soc.* **1996**, *118*, 2245.

(8) Schowen, R. L. *Prog. Phys. Org. Chem.* **1972**, *9*, 275.

(9) Oppenheimer, N. J.; Handlon, A. L. In *The Enzymes*; Sigman, D. S., Ed.; Academic Press: San Diego, CA, 1992; p 453.

(10) Wiberg, K. B.; Morgan, K. M.; Maltz, H. *J. Am. Chem. Soc.* **1994**, *116*, 11067.

(11) Gębicki, J.; Marcinek, A.; Adamus, J.; Paneth, P.; Rogowski, J. *J. Am. Chem. Soc.* **1996**, *118*, 691.

(12) Marcinek, A.; Rogowski, J.; Adamus, J.; Gębicki, J.; Platz, M. S. *J. Phys. Chem.* **1996**, *100*, 13539.

(13) Marcinek, A.; Zielonka, J.; Gębicki, J. Manuscript in preparation.

(14) Levanon, H.; Neta, P. *Chem. Phys. Lett.* **1980**, *70*, 100.

(15) Anne, A.; Hapiot, P.; Moiroux, J.; Neta, P.; Savéant, J.-M. *J. Am. Chem. Soc.* **1992**, *114*, 4694.

(16) Neta, P. *J. Phys. Chem.* **1979**, *83*, 3096.

(17) Anne, A.; Hapiot, P.; Moiroux, J.; Neta, P.; Savéant, J.-M. *J. Phys. Chem.* **1991**, *95*, 2370.

(18) Adamus, J.; Rogowski, J.; Michalak, J.; Paneth, P.; Gębicki, J.; Marcinek, A.; Platz, M. S. *J. Phys. Org. Chem.* **1993**, *6*, 254.

(19) van Eikeren, P.; Grier, D. L. *J. Am. Chem. Soc.* **1977**, *99*, 8057.

(20) van Eikeren, P.; Kenney, P.; Tokmakian, R. *J. Am. Chem. Soc.* **1979**, *101*, 1402.

(21) Moiroux, J.; Elving, P. J. *J. Am. Chem. Soc.* **1980**, *102*, 6533.

(22) Anderson, A. G., Jr.; Berkelhammer, G. *J. Am. Chem. Soc.* **1958**, *80*, 992.

(23) Buxton, G. V.; Greenstock, C. L.; Helman, W. P.; Ross, A. B. *J. Phys. Chem. Ref. Data* **1988**, *17*, 513.

(24) Neta, P.; Huie, R. E.; Ross, A. B. *J. Phys. Chem. Ref. Data* **1988**, *17*, 1027.

(25) Mohan, H.; Srividya, N.; Ramamurthy, P.; Mittal, J. P. *J. Chem. Soc., Faraday Trans.* **1996**, *92*, 2353.

(26) Karolczak, S.; Hodyr, K.; Łubis, R.; Kroh, J. *J. Radioanal. Nucl. Chem.* **1986**, *101*, 177.

(27) Gębicki, J.; Marcinek, A.; Rogowski, J. *Radiat. Phys. Chem.* **1992**, *39*, 41.

(28) Becke, A. D. *J. Chem. Phys.* **1993**, *98*, 5648.

(29) Lee, C.; Yang, W.; Parr, R. G. *Phys. Rev. B* **1988**, *37*, 785.

(30) Frisch, M. J.; Trucks, G. W.; Schlegel, H. B.; Gill, P. M. W.; Johnson, B. G.; Robb, M. A.; Cheeseman, J. R.; Keith, T.; Petersson, G. A.; Montgomery, J. A.; Raghavachari, K.; Al-Laham, M. A.; Zakrzewski, V. G.; Ortiz, J. V.; Foresman, J. B.; Cioslowski, J.; Stefanov, B. B.; Nanayakkara, A.; Challacombe, M.; Peng, C. Y.; Ayala, P. Y.; Chen, W.; Wong, M. W.; Andres, J. L.; Replogle, E. S.; Gomperts, R.; Martin, R. L.; Fox, D. J.; Binkley, J. S.; Defrees, D. J.; Baker, J.; Stewart, J. P.; Head-Gordon, M.; Gonzalez, C.; Pople, J. A. *Gaussian 94*, revisions B1 and D4; Gaussian, Inc.: Pittsburgh, PA, 1995.

(31) For a description of the DFT methods implemented in the Gaussian program, see the following. Johnson, B. G.; Gill, P. M. W.; Pople, J. A. *J. Chem. Phys.* **1993**, *98*, 5612.

(32) Andersson, K.; Roos, B. O. In *Modern Electronic Structure Theory*; World Scientific: Singapore, 1995; Part 1, Vol. 2, p 55.

(33) Andersson, K.; Blomberg, M. R. A.; Fülscher, M. P.; Kellö, V.; Lindh, R.; Malmqvist, P.-Å.; Noga, J.; Olson, J.; Roos, B. O.; Sadlej, A.; Siegbahn, P. E. M.; Urban, M.; Widmark, P.-O. *MOLCAS*, versions 3 and 4; University of Lund: Sweden, 1994.

(34) Pierloot, K.; Dumez, B.; Widmark, P.-O.; Roos, B. O. *Theor. Chim. Acta* **1995**, *90*, 87.